

Slidegate Dithering Effects on Transient Flow and Mold Level Fluctuations

Slidegate dithering has been implemented in the continuous casting of steel to improve the control of flowrate by oscillating the slidegate back and forth at a particular stroke and frequency. The continuous motion prevents sticking and may reduce clogging. However, slidegate dithering also causes transient variations in fluid flow inside the submerged entry nozzle (SEN) as well as in the mold region.¹ This has a direct impact on mold level fluctuations, which are crucial to the quality of the final products. Mold level fluctuations are one of the most significant mechanisms responsible for mold slag entrainment and the formation of surface defects and other quality problems in the final product, such as slivers.²

Previous work on dithering has generally focused on measurement of mold level.^{3–5} Control systems must be altered to maintain constant average flowrate and stable mold level, and special control algorithms have been developed to accomplish this.^{3–5} Recently, dithering has been investigated using computational models,¹ calculating mold level using a simple pressure method with a fixed wall condition imposed at the slag/steel interface. With a low-frequency dithering practice (0.4 Hz) and a 1,840-mm mold width, the periodic mold level change was found to be dominated by mass

conservation of the liquid steel. The predictions of mold level fluctuations using the pressure method were compared favorably with plant measurements from the dithering trial. This method has thus been found to be reasonably accurate for relatively small surface waves. For larger waves capable of causing sloshing, the effects of gravity need to be incorporated, so a free-surface tracking/capturing algorithm, such as the volume of fluid (VOF) method,⁶ has to be implemented in the model.

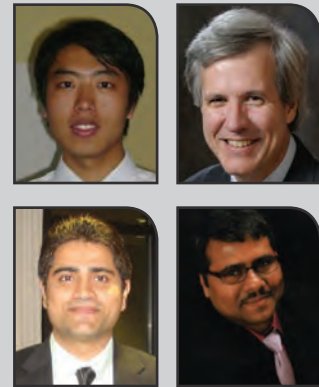
In this work, models were developed, validated and combined together as a system to predict 3D transient turbulent flow in the nozzle and mold region, together with argon gas effects using an efficient new free-surface tracking of this complicated flow system. In addition, a simple analytical model based on mass conservation of the liquid was developed and validated. The detailed mechanism of how mold flow activates the mold sloshing was revealed, and parametric studies were conducted to study the effects of casting speed, mold width and dithering stroke on mold level fluctuations.

Plant Measurements

During recent trials conducted at ArcelorMittal Indiana Harbor No. 3 Steel Producing (3SP), various slidegate dithering

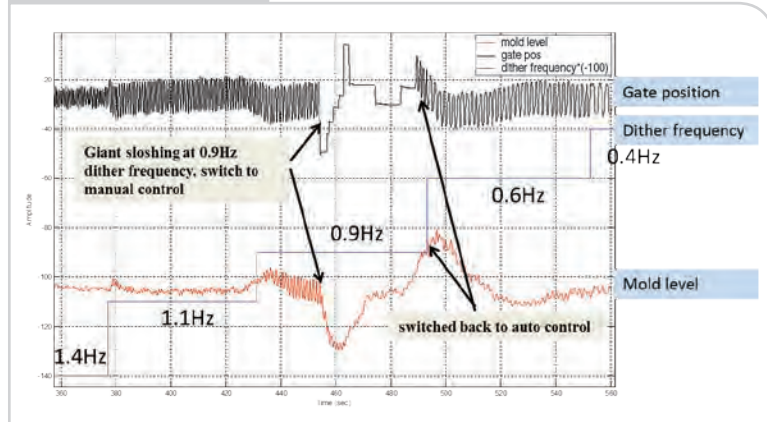
The effects of slidegate dithering on surface flow behavior during continuous casting are investigated via mathematical modeling and plant trial measurements. A transient turbulent flow model with a new free-surface tracking algorithm using a dynamic mesh was developed, validated and applied to match different measured level fluctuation histories.

Authors



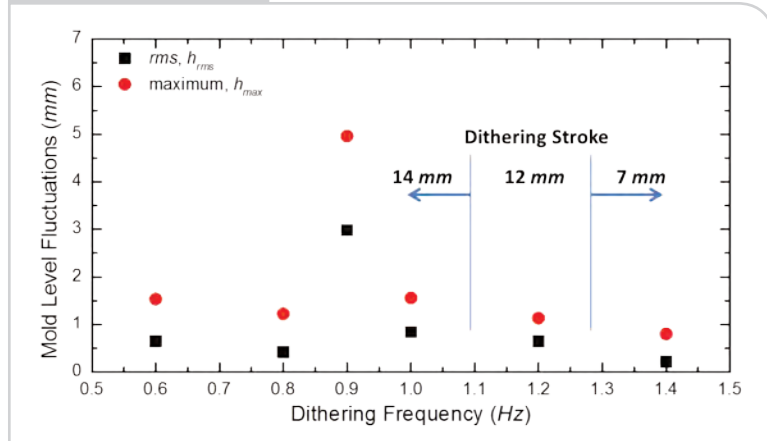
Rui Liu (top row, left) research assistant; Brian G. Thomas (top row, right), C.J. Gauthier Professor of Mechanical Engineering (bgthomas@illinois.edu), Department of Mechanical Science and Engineering, University of Illinois at Urbana-Champaign, Urbana, Ill., USA; Love Kalra (bottom row, left), senior engineer (love.kalra@arcelormittal.com), ArcelorMittal No. 3 Steel Producing, East Chicago, Ind., USA; Tathagata Bhattacharya (bottom row, right), research engineer (tathagata.bhattacharya@arcelormittal.com), ArcelorMittal Global R&D – East Chicago, East Chicago, Ind., USA; and Aloka Dasgupta (not pictured), senior process engineer, ArcelorMittal No. 3 Steel Producing, East Chicago, Ind., USA

Figure 1



Dithering trials with mold level measurements at ArcelorMittal Indiana Harbor No. 3 Steel Producing (3SP).

Figure 2



Influence of dithering frequency on mold level fluctuations.

conditions were investigated (dithering frequency and stroke) for different casting speeds and mold widths. The eddy current sensor recorded the mold level at the mold quarter point, and an example of the results is plotted in Figure 1. Large sloshing waves were observed in the mold with a 1,840-mm (72.5-inch) slab width by mold operators at a dithering frequency of 0.9 Hz, which prompted switching to manual level control for safety. The gravity wave that caused this large-amplitude sloshing in the mold has not been predicted in previous models.¹

The effect of dithering frequency on mold level fluctuations is further plotted in Figure 2. Both the maximum and the root mean square (rms) of the measured mold level fluctuations are calculated and presented. For most frequencies (other than 0.9 Hz), the mold level fluctuations are affected only by the dithering stroke, and dithering frequency has little effect. However, when the dithering frequency was

0.9 Hz, (1,840-mm width), both the rms and maximum mold level fluctuations jumped to about 4–5 times larger than those from all the other cases. These giant mold level fluctuations (over 10 mm from peak to valley) were identified to be caused by severe mold sloshing waves. The purpose of this paper is to create and apply computational and analytical models to investigate the effect of dithering on mold level fluctuations, including the prediction and understanding of the sloshing mechanism that causes the giant level fluctuations.

Mold Sloshing Estimation

Sloshing in the mold resembles that in a rectangular tank, which has been well investigated by previous researchers.^{7–8} The natural frequency for the tank sloshing problem is given by Equation 1,⁷ and pictured in Figure 3.

$$f_{i,j}^2 = \frac{g}{4\pi} \sqrt{\left(\frac{i}{a}\right)^2 + \left(\frac{j}{b}\right)^2} \tanh \left[\pi h \sqrt{\left(\frac{i}{a}\right)^2 + \left(\frac{j}{b}\right)^2} \right] \quad (\text{Eq. 1})$$

where

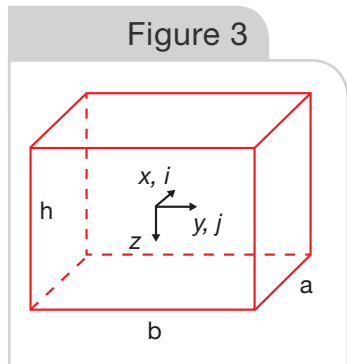
f (Hz) is the natural frequency,
 i and j are sloshing mode indices along the x and y-axis respectively,
 a , b and h (m) are the tank dimensions in the x, y and z-directions, respectively, and
 g is gravity acceleration (9.81 m/second²).

The sloshing frequencies for different mold dimensions using Equation 1 are plotted in Figure 4. Because the caster is deep, the tanh term in Equation 1 is about 1, so it can be neglected. From Figure 4, for a slab width of 1,840 mm (72.5 inches), the first-mode, half-width from SEN to NF (0,1), or the second-mode, full-width from NF to NF (0,2), the sloshing frequency is 0.92 Hz in both cases, which is very close to the sloshing frequency observed in the plant. Thus, Figure 4 shows the mold width/dithering frequency combinations to avoid. Other specific frequencies to avoid are 1.17 Hz for a 1,143-mm (45-inch)-wide slab, 1.1 Hz for a 1,270-mm (50-inch)-wide slab, 1.0 Hz for a range of slab widths between 1,524 mm (60 inches) and 1,650 mm (65 inches).

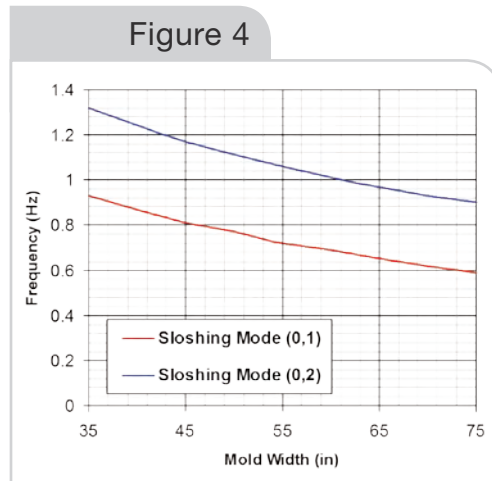
Model Description and Validation

A system of models has been developed to handle each of the complex phenomena associated with the effect of slidegate dithering on transient, turbulent, multi-phase flow in the nozzle and mold and the associated mold level fluctuations, and is presented in Figure 5.

First, the liquid steel flowrate through the SEN is calculated based on the position of the slidegate recorded during dithering by adapting a flowrate model from a previous study.¹ Next, the 3D flow pattern in the SEN and mold are calculated by solving the transient Navier-Stokes equations using the standard $k-\omega$ model for turbulence with the CFD package, FLUENT. In order to model the gravity waves, a new free-surface tracking algorithm with an adaptive dynamic mesh is employed to compute the motion of the mold top surface. A simple analytical model based on the liquid steel mass conservation was developed to calculate the average mold level change during the dithering process. All of these models were validated with experimental measurements, and then applied to investigate the transient flow pattern evolution and mold level fluctuations during slidegate dithering.



Schematic of sloshing mode indices.

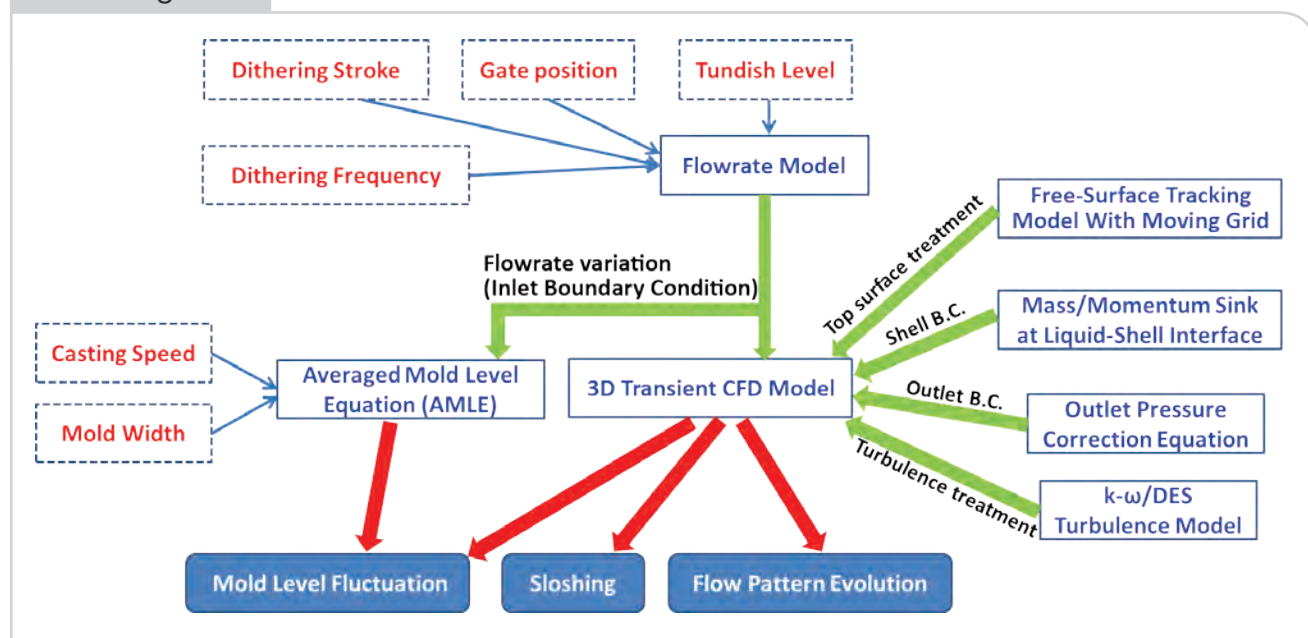


Mold natural frequency curves.

Flowrate Model — The liquid steel flowrate into the upper tundish nozzle (UTN) and SEN varies with the slidegate position during dithering. In previous work,¹ the flowrate through a water model was measured as a function of slidegate opening position and found to match the following the Bernoulli equation (Equation 2) for a 90-mm-diameter SEN with 75-mm slidegate bore. Parameter C in Equation 2 is the clogging factor, which is set to 0 in the current study. The match with measurements is shown in Figure 6.

Note that fluid density does not appear in Equation 2: this equation also describes liquid steel flowrate in the SEN. This model was used in this work

Figure 5



Model system for dithering process simulations.

Equation 2

$$Q_{SEN} = A_{eff} \sqrt{\frac{2g(H_1 + H_2)}{\left(\left(\frac{A_{SEN}}{A_{port}} - 1\right)^2 + f \frac{L_{SEN}}{D_{SEN}} + \left(\frac{1}{\mu} - 1\right)^2 \left(\frac{A_{SEN}}{A_{GAP}}\right)^2 + \left(\frac{A_{SG}}{A_{GAP}} - \frac{A_{GAP}}{A_{SG}}\right)^2 \left(\frac{A_{SEN}}{A_{SG}}\right)^2 + \left(\frac{A_{SEN}}{2A_{port}}\right)^2 + C}}}$$

where

Q_{SEN} is the calculated fluid volumetric fluid flowrate in UTN/SEN,

H_1 (m) is the distance between the tundish level and bottom of the tundish,

H_2 (m) is the distance from UTN upper edge to the upper edge of SEN port exit,

g is the gravitational acceleration (m/second²),

A_{SEN} (m²) is the SEN inner cross-section area,

A_{port} (m²) is the area of the port exit projected to the liquid steel jet direction,

f is the friction factor for turbulent flow in a circular pipe, with an estimated value of 0.075 from Moody's chart,

L_{SEN} (m) is the SEN length,

D_{SEN} (m) is the SEN inner diameter (90 mm in water model, 80 mm in caster),

μ is the coefficient of contraction,

A_{SG} (m²) is the area of the slidegate when it is fully opened and

A_{GAP} (m²) is the gap opening area projected in the casting direction, which depends on measured slidegate position.

to generate the boundary conditions at the UTN inlet for both models of mold surface level.

3D Transient CFD Model for SEN/Mold Flows — The computational model of transient turbulent flow is described in this section, including the governing equations, the geometry and mesh of the domain, and the boundary conditions.

Governing Equations: The governing equations for the current transient fluid flow model include the mass-conservation Equation 3, and the momentum-conservation Equation 4, which must consider the moving mesh velocity.

$$\nabla \cdot (\rho(\mathbf{v} - \mathbf{v}_g)) = 0 \quad (\text{Eq. 3})$$

$$\frac{\partial(\rho\mathbf{v})}{\partial t} + \nabla \cdot (\rho\mathbf{v}(\mathbf{v} - \mathbf{v}_g)) = -\nabla p + \nabla \cdot (\mu\nabla\mathbf{v}) + \rho\mathbf{g} \quad (\text{Eq. 4})$$

In Equations 3 and 4, \mathbf{v}_g is the node velocity in the dynamic mesh region, which was defined in the upper (moving mesh) layer of the fluid bulk domain, and is simply 0 elsewhere in the domain. Further equations for conservation of the argon

gas mass and momentum, and the two extra transport equations for the parameters in the k- ω turbulence model are given elsewhere.⁹ Details of the DES model can be found in Reference 10.

Computational Domain Geometry and Mesh:

Half of the full slidegate, nozzle and mold region is taken as the computational domain, due to symmetry, as shown in Figure 7a. The mold domain has been divided into two sub-domains, an upper 10-cell layer (100 mm) for the dynamic mesh region and a lower layer (2,400 mm) for the bulk of the fluid with fixed mesh (shown in Figure 7a). This division of the fluid bulk is done for computational efficiency, as only the mesh near the meniscus must be smoothed to preserve mesh quality. To make the most coupled parts of the model parallelizable for best computational efficiency, the upper layer of the mold bulk is assigned to a single processor, while the rest of the domain is split between five processors. Thus, slow mesh updating between processors is avoided in each iteration, and computational efficiency is better.

A mesh of 1 million hexahedral cells was adopted for all simulations, as shown in Figure 7b–c. Close-ups are shown around the slidegate region in Figure 7b, and around the free-surface region near the SEN and mold in Figure 7c.

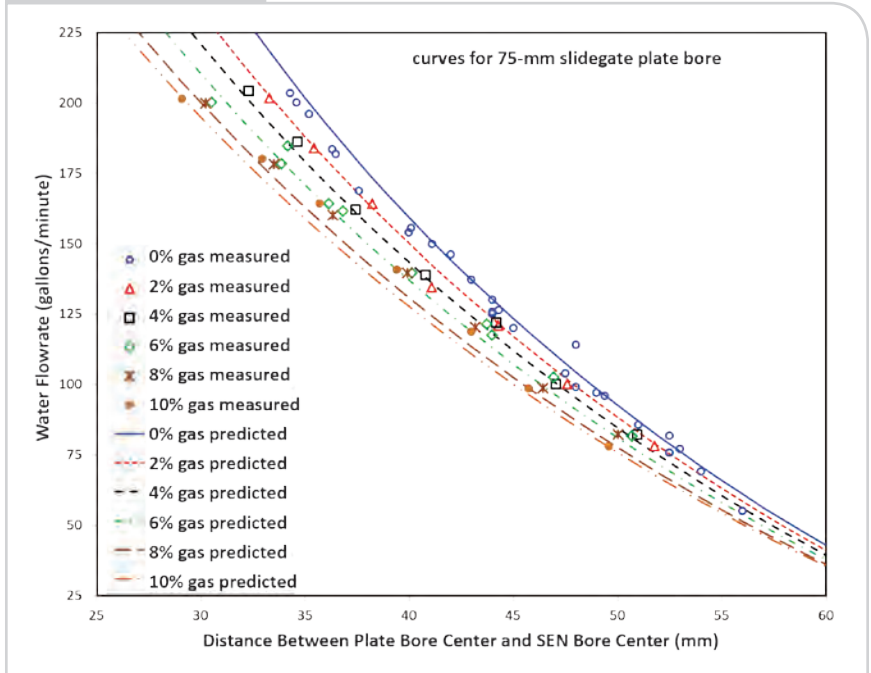
Boundary Conditions — The boundary conditions (BCs) for the dithering process simulations include the UTN inlet for liquid steel, the mold top surface, solidified shell, and outlet from the domain bottom. For each of these boundaries, a special sub-model was applied, as detailed in this section.

UTN Inlet BC With Liquid Steel Flowrate History: Liquid steel flowrate from the flowrate model is converted to a prescribed-velocity history boundary condition at the UTN inlet. Usually this velocity could be calculated from the casting speed. However, the dithering process causes periodic variations in flowrate/velocity due to the periodic change of slide-gate position. Thus, this flowrate history is calculated using Equation 2.

Shell BC With Mass/Momentum Sinks: Near the liquid/shell interface, liquid steel continuously solidifies into a solid shell, which moves downward at the constant casting speed. The shape of the shell does not change with time, when viewed in an Eulerian frame of reference. Thus, in the current work, a moving-wall boundary condition (at the casting speed) is applied at the shell boundary. To account for liquid steel exiting the domain across this wall, mass and momentum sinks are incorporated via a user-defined function (UDF). A detailed derivation of these sink terms is found in Reference 11.

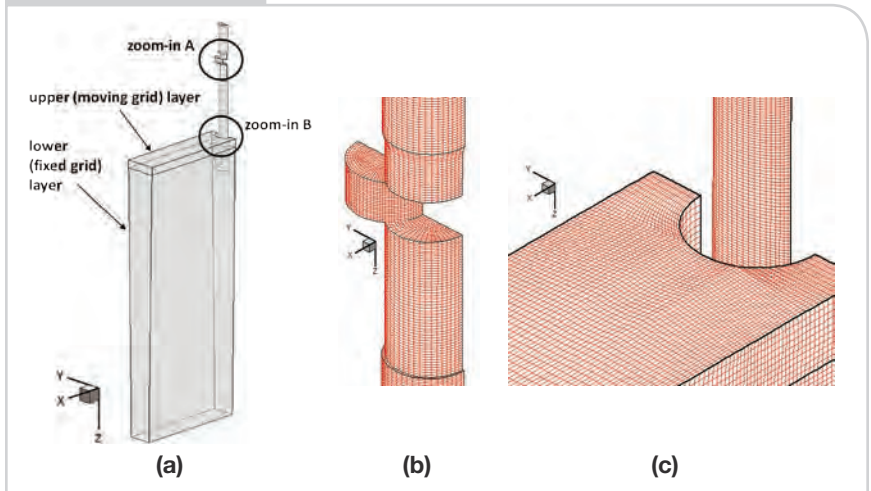
Domain Top Surface BC: Motion of the mold top surface (slag/steel interface) is modeled with a new free-surface tracking method, based on a moving grid technique by Muzaferija and Perić¹² that is combined with a dynamic mesh capability within ANSYS-FLUENT¹³ and implemented via a UDF. This new method is validated with an analytical solution to a tank sloshing problem, and is

Figure 6



Comparison of flowrate model results with water model experiments data.¹

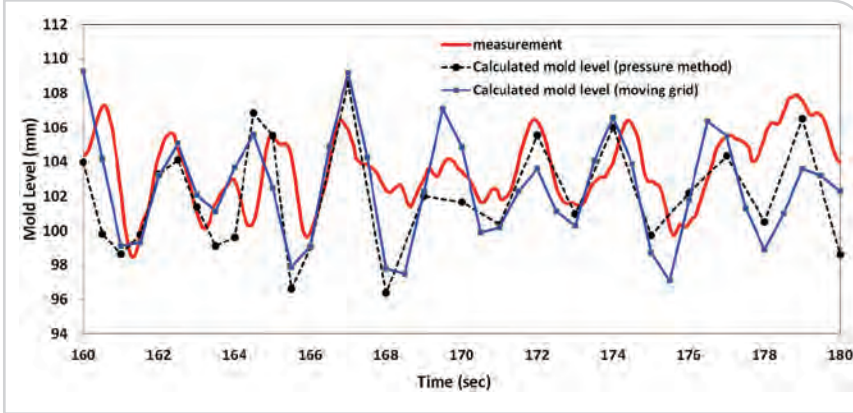
Figure 7



Domain geometry and mesh setup: domain geometry (a), zoomed-in region A (b) and zoomed-in region B (c).

described elsewhere.¹¹ The boundary conditions on the slag/steel interface (domain top surface) require no penetration of fluid through the slag/steel interface (kinematic BC) and all forces in equilibrium at the free surface (dynamic BC). The kinematic boundary condition is given by Equation 5, where \mathbf{v} is the fluid velocity and \mathbf{v}_s is the free surface velocity.

Figure 8



Free-surface model validation of mold level fluctuation with an argon-steel two-phase mold flow simulation.

$$\left[(\mathbf{v} - \mathbf{v}_s) \cdot \mathbf{n} \right]_s = 0 \quad (\text{Eq. 5})$$

At the mold top surface, a liquid flux layer that floats on the liquid steel surface adds a roughly constant pressure to the slag/steel interface. The thickness of the top liquid flux layer varies with position on the surface. Considering the unsteady nature of the slag/steel interface motion, it is assumed that the liquid flux and powder layers do not have enough time to re-distribute during the dithering cycle, so it is reasonable to assume a constant thickness (pressure) on top of liquid steel. Furthermore, the turbulence model is designed to filter (average) local instantaneous small-scale turbulent eddies, so the curvature of the domain top surface is small enough to neglect surface tension effects. With these assumptions, the dynamic boundary condition is given by Equation 6:

$$p = p_0 + \rho_{flux} g h_{flux} + \mathbf{n} \cdot \mu \left[\nabla \mathbf{v} + (\nabla \mathbf{v})^T \right] \cdot \mathbf{n} \quad (\text{Eq. 6})$$

where

the pressure p_0 in the right-hand side of Equation 6 is atmospheric pressure (0.101 MPa),
 ρ_{flux} is 3,000 kg/m³, g is 9.81 m/second²,
 h_{flux} is the constant (20-mm) thickness of the flux and powder layers,
 \mathbf{v} is the velocity vector at free surface and
 \mathbf{n} is the normal unit vector of the local free surface.

Domain Outlet Pressure BC:

Hydraulic pressure of the liquid steel at the domain outlet is usually adopted for mold flow simulations with fixed wall boundaries at the top surface. When a pressure boundary condition such as Equation 6 is applied at the domain top surface, however, a more accurate outlet boundary is needed. In this work, this pressure boundary condition is modified to ensure that the current liquid steel flowrate is matched at the domain outlet. The correction to the outlet boundary pressure is given by Equation 7:

$$d\bar{p} = \rho \frac{\left(\frac{Q_T}{WT} \right)^2 - \left(\frac{Q_C}{WT} \right)^2}{2} \quad (\text{Eq. 7})$$

where

Q_T is the target volumetric flowrate of liquid steel in the system,
 Q_C is the current volumetric flowrate at the domain outlet and
 W and T are the slab width and thickness at the domain bottom outlet.

This equation is based on Bernoulli's equation, as derived in Reference 11. This modification of boundary pressure is crucial to a successful dithering simulation, because the motion of the slag/steel interface can be accurately computed only if the outlet flowrate is correct and properly conserves mass in the entire system.

Model Validation With Plant Measurements — The entire 3D multi-phase computational model, including the new free-surface prediction method, was validated by comparing with plant measurements with dithering. Simulations were performed for the conditions of Liu et al.,¹ which include dithering (14 mm stroke, 0.4 Hz frequency), 1.0 m/minute casting speed, 1,840 mm width, and 6% argon gas in the hot condition. The predictions from the two different free-surface models are compared in Figure 8 with the mold level sensor measurements. As observed in Figure 8, both methods match reasonably well with the experiment measurements, and this new numerical model is again validated.

Model Validation With DES

Model — Before performing a simulation of transient behavior such as dithering, the CFD model is first run for ~10 seconds (in physical time) until the flow is established. Instantaneous results using two different turbulence models, the k- ω model and the detached eddy simulation (DES) model, are compared in this section. The k- ω model resembles the standard k- ϵ two-equation model for unsteady Reynold's averaged Navier-Stokes (U-RANS) simulation.⁹ The DES performs large eddy simulation (LES) in the fluid bulk region to capture the local instantaneous turbulent eddies, and adopts a RANS wall function close to the no-slip wall to resolve the details of the turbulent boundary layer fluctuations with less computational effort than LES.¹⁰

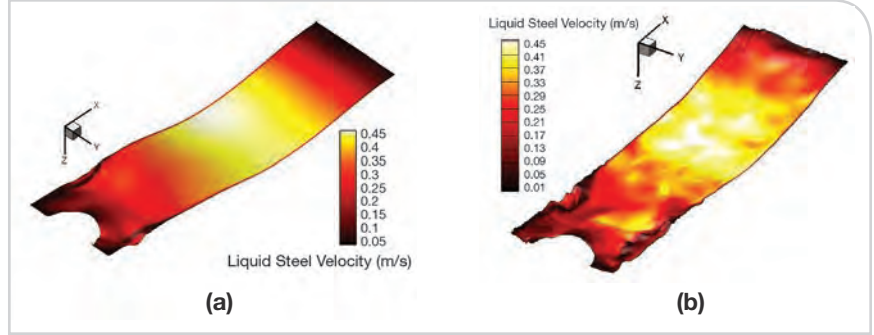
The free-surface and velocity results from these two models are compared in Figure 9. The k- ω model generates the expected smoothed top-surface profile, while DES gives an instantaneous surface shape. Both simulations give a lower surface level and higher surface velocity around the quarter mold region, while the top surface rises near the SEN and the narrowface, with a lower surface velocity.

Figure 10a shows the zoomed-in deformed shape of the mold top surface during constant casting speed without dithering from the DES model. Note that the length scale in the vertical (z-) direction is stretched by 5 times for easier visualization of the shape. Small vortices and wrinkles appear, especially near the SEN outer perimeter. The mold level rises close to the SEN, due to the impingement of the liquid steel stream flowing toward the SEN. Velocity vectors along the free surface are plotted in Figure 10b. Recirculation regions are observed near both sides of the SEN, which cause dimples (depressions) to form on the free surface.

Averaged Mold Level Equation

(AMLE) — Changes of the average mold level can be derived by performing a mass balance on the steel flowrate history averaged over the cross-sectional area

Figure 9



Comparison of simulated mold top surface morphologies by different turbulence models: by k- ω model (a) and by DES model (b).

of the entire computational domain. Balancing the flowrate variations through the SEN with changes in average surface level in the mold leads to Equation 8.

$$V_l \left(A_l - \frac{\pi}{4} D_o^2 \right) + V_c A_l = Q_{SEN} \quad (\text{Eq. 8})$$

where

V_l (m/second) is the average vertical velocity of the liquid steel surface level in the mold,
 A_l (m²) is the slab cross-section area at meniscus,
 D_o (m) is the outer diameter of the SEN and
 V_c (m/second) is the casting speed.

Equations 9 –10

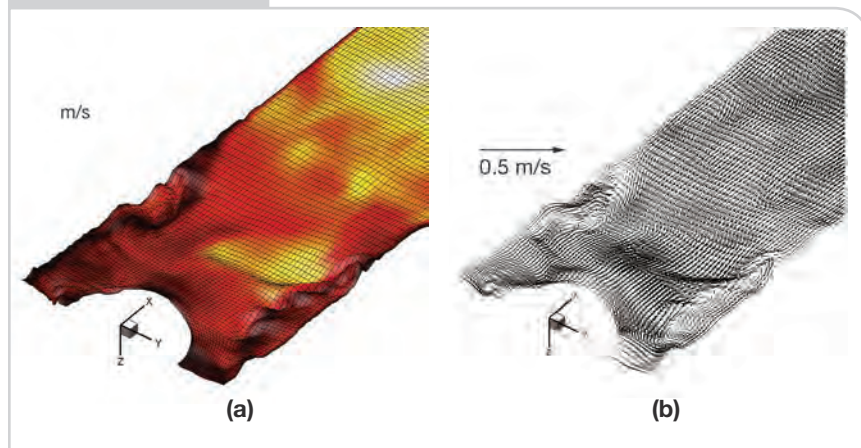
$$h(t) = \int_{t_0}^t \left(\frac{Q_{SEN}}{\alpha_A A_l} - \frac{V_c}{\alpha_A} \right) dt' + h_0 = \frac{1}{\alpha_A A_l} \int_{t_0}^t Q_{SEN} dt' - \frac{1}{\alpha_A} \int_{t_0}^t V_c dt' + h_0, \quad \alpha_A = 1 - \frac{\pi D_o^2}{4WT} \quad (\text{Eq. 9})$$

$$h_n = \frac{1}{\alpha_A A_l} \sum_{i=0}^n Q_{SEN}(t_i) \Delta t - \frac{1}{\alpha_A} V_c (t_n - t_0) + h_0 \quad (\text{Eq. 10})$$

where

t_n (second) is the time at time step n,
 h_n (mm) is the average mold level at time t_n , relative to h_0 at t_0 measured at the start of the time interval,
 Q_{SEN} (m³/second) is volumetric flowrate from Equation 2, based on the measured slidegate position,
 W (m) is the mold width and
 T (m) is the mold thickness.

Figure 10



Zoomed-in view of free surface close to the SEN calculated using DES (length magnified by 5x along z-axis: free-surface morphology with mesh deformation (a), and top surface liquid steel velocity close to the SEN (b).

$$h_{rms} = \sqrt{\overline{h'^2}} = \sqrt{\frac{\sum_{i=1}^N (h_i - \bar{h})^2}{N}} \quad (\text{Eq. 11})$$

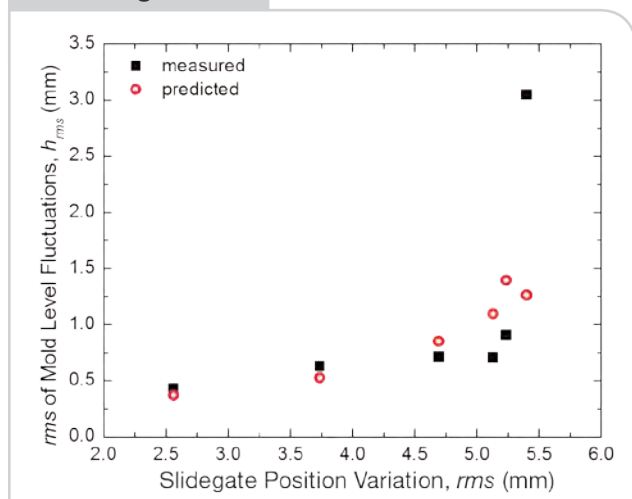
where

h (mm) is mold level,
 \bar{h} is time average and
 N is the total number of sampling points (~1,000, taken over a time interval of 10 seconds).

To validate this model, it is first applied to predict average mold level fluctuation results for cases with plant measurements. The measured and predicted mold level fluctuations are compared in Figure 11.

In most of the cases, the predicted mold level fluctuations reasonably match the measurements. However, in the case with a 5.5-mm slidegate position variation, a huge deviation appears. This is the case where severe mold sloshing was observed. In this case, the averaged mold level fluctuations are caused by gravity waves, so the prediction based on a mass balance on the flowrate cannot reflect the real slag/steel interface behavior. Thus, the AMLE model is accurate, unless giant sloshing occurs.

Figure 11



Comparison between measured and predicted mold level fluctuations.

Integrating the velocity V_l in Equation 8 gives the mold level $h(t)$ in Equation 9, integrated numerically to Equation 10.

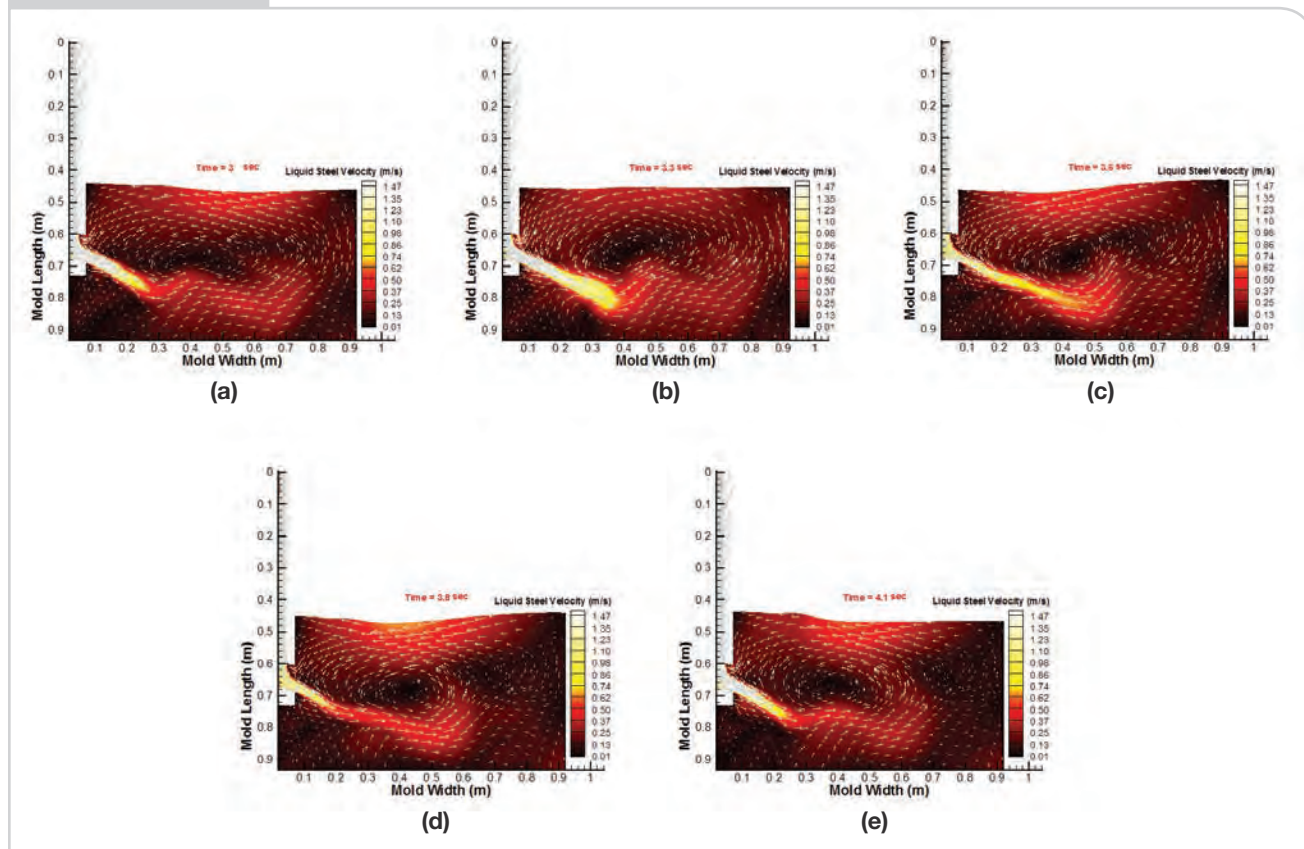
Since the averaged mold level position is an integral of the SEN liquid steel flowrate over time, a sudden change of the flowrate takes time to affect the mold level. Similar approaches used to estimate mold level fluctuations can also be found in previous studies, where researchers used the predicted mold level fluctuations to calibrate their control algorithms.^{3,5} To quantify the fluctuations in mold level, Equation 11 defines the standard deviation or rms of the mold level fluctuation relative to the mean level (\bar{h}). Larger h_{rms} indicates higher chances of quality problems:

Results and Discussion

This section presents the transient flow pattern and evolution of the slag/steel interface for the dithering process conditions that caused mold sloshing. The predicted mold level fluctuations are compared with plant measurements. A parametric study is then conducted to investigate the average mold level fluctuations during typical dithering processes. The mold dimensions for this study are 1,840-mm width and 254-mm thickness. The SEN has an 80-mm inner bore diameter, a roof-type bottom, and 80-mm-diameter ports with a downward angle of 15°, 143-mm submergence depth and 75-mm slidegate plate diameter. These conditions are consistent with those used to generate the flowrate curves in Figure 6. A total flowrate of 1 standard liter per minute (slpm) argon was injected into the UTN, corresponding to about 1% gas volume fraction in the hot condition. This is small enough that single-phase flow was assumed in the current simulation.

Simulation results of the transient flow pattern evolution for the mold sloshing case with 0.9-Hz

Figure 12



Transient liquid steel flow pattern evolution during one dithering cycle for the mold sloshing case: flow time = 3 seconds (a), flow time = 3.3 seconds (b), flow time = 3.6 seconds (c), flow time = 3.8 seconds (d), and flow time = 4.1 seconds (e).

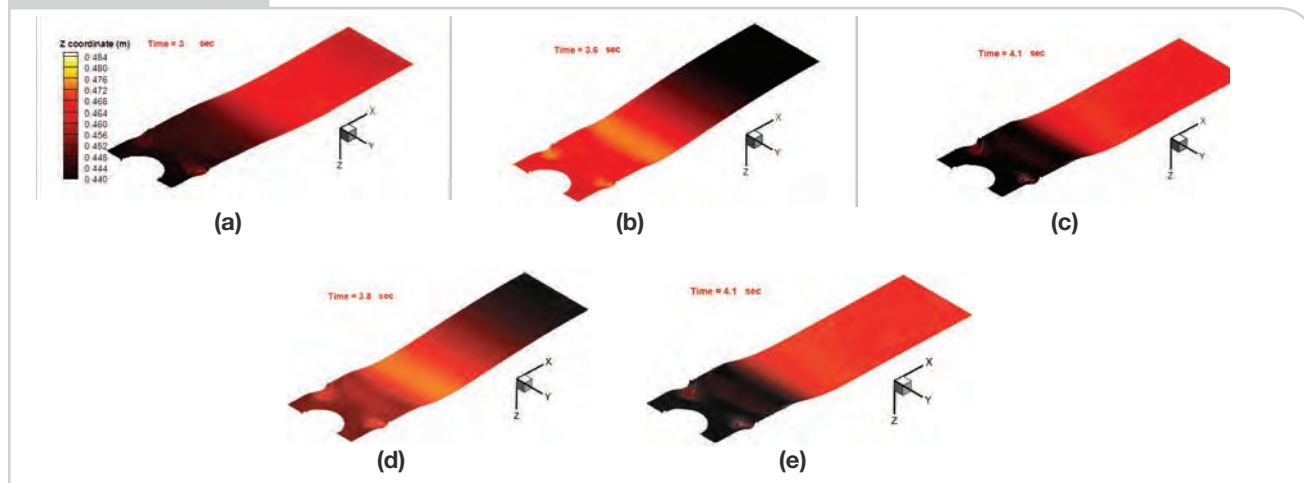
dithering frequency and 14-mm dithering stroke, and 1.0 m/minute casting speed are shown in Figures 12a–e. Approximately five dithering cycles were simulated (starting from 0 seconds), and the cycle from 3.0 to 4.1 seconds is presented in Figures 12 and 13. At time 3.0 seconds at the start of a dithering cycle, the strength of the liquid steel jet starts to increase. The mold top-surface level is higher close to the SEN, and lower at the narrowface. At 3.3 seconds, the jet grows stronger, and the recirculation velocity around the upper roll is accelerated. During this time, the mold surface level near the SEN decreases, while the surface level at the mold narrowface increases. The slag/steel interface is relatively flat by this time. At 3.6 seconds, the established jet starts to decrease in strength, due to the upstream closing of the slidegate. At this moment, the surface level at the mold narrowface reaches its peak. At 3.8 seconds, the jet is at its weakest, and the mold surface level near the SEN is still increasing, while the level at the mold narrowface continues to decrease. When the time reaches 4.1 seconds, the surface level at the SEN has risen to its highest point and begins to drop, while the level at the narrowface starts to increase from its lowest point.

At the same time, the liquid steel jet strength starts to increase, and the next dithering cycle begins.

Throughout each dithering cycle, the liquid steel jet leads a wobbling path toward the mold narrowface due to the flowrate variation, and the flow pattern in the mold region remains double-roll. The duration of this large-scale eddy is long enough that the change of inlet liquid steel flowrate does not alter the flow pattern. The recirculation velocity in the upper roll is accelerated and slowed down periodically. When the dithering frequency matches the mold natural frequency, as in this simulation, the increase of the jet strength accelerates the rising velocity of the mold surface level at the narrowface. In this manner, the kinetic energy increase from the jet outweighs the energy dissipated by the viscous effects. Thus, mold sloshing gets energized and magnified in every dithering cycle.

The 3D motion of the mold top surface is shown in Figures 13a–e, where the contours indicate the local level. Dark regions indicate high surface levels, while red regions have lower levels. From 3.0 to 3.3 seconds, surface level drops near the SEN and increases near the narrowface. At 3.3 seconds, the surface levels are

Figure 13



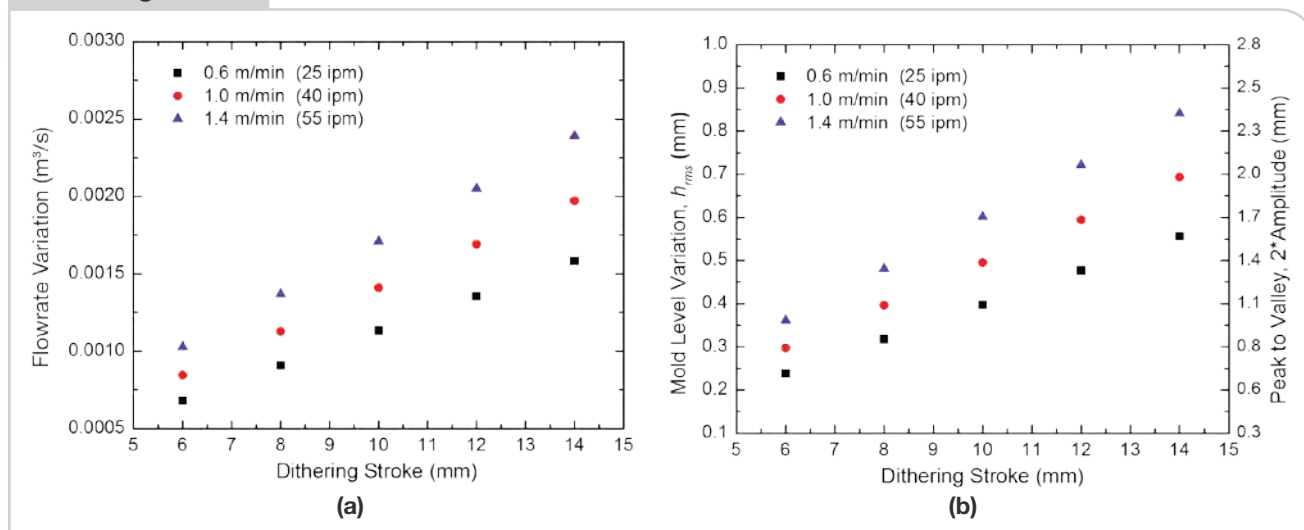
Mold top surface behavior during one dithering cycle: 3 seconds (a), 3.3 seconds (b), 3.6 seconds (c), 3.8 seconds (d), 4.1 seconds (e).

almost even. Then the level at the narrowface starts increasing, due to the increased momentum of the liquid steel jet flowing up the narrowface. At 3.6 seconds, surface level reached its maximum at the narrowface. For the next 0.5 seconds, a ~35-mm-high wave flows across the top surface toward the SEN, finally producing a maximum surface level at the SEN at 4.1 seconds. This time coincides with the beginning of the next dithering cycle, which causes the process to repeat in an amplified manner during the next dithering cycle.

Parametric Studies — For dithering practices which do not activate the gravity-wave sloshing mechanism, mass conservation dominates the mold level

fluctuations, as discussed previously.¹ Thus, parametric studies using the AMLE model were conducted to investigate the effects of casting speed and dithering stroke on flowrate variations and mold level fluctuations for a 1,840-mm mold width. The flowrate variations are calculated using Equation 2 and are presented in Figure 14a. The mold level variations (rms) are calculated with Equations 8–11 and shown in Figure 14b. Note that the actual peak-to-valley mold level fluctuations are around 3 times the mold level rms values calculated, as shown on the right axis in Figure 14b. Five dithering strokes were modeled — 6, 8, 10, 12 and 14 mm — at three different casting speeds, 0.6, 1.0 and 1.4 m/minute (25, 40 and 55 ipm).

Figure 14



Effects of dithering stroke and casting speed on flowrate variation and mold level fluctuation: correlation between flowrate variation and stroke (a), and mold level fluctuation dependence (b).

Effects of Dithering Stroke — The effects of dithering stroke are shown in Figure 14 for different casting speeds. Liquid steel flowrate changes during dithering according to the dithering stroke. This causes the average mold levels to vary, while casting speed is constant. Increasing dithering stroke increases these flowrate variations, which in turn raises mold level fluctuations. Specifically, increasing dithering stroke from 6 to 14 mm increases flowrate variations by ~140%, causing level fluctuations to rise from ~0.25 to ~0.55 mm (rms) for low (0.6 m/minute) casting speed, from ~0.3 to ~0.7 mm for medium (1.0 m/minute) casting speed, and from ~0.35 to ~0.85 mm for high (1.4 m/minute) casting speed.

Effects of Casting Speed — The effects of casting speed are shown in Figure 14 for different dithering strokes. As casting speed increases, the flowrate variations through the UTN increase as well. At lower casting speeds, the rms of mold level fluctuation is less than 0.7 mm, even with a high dithering stroke. When casting speed increases to 1.4 m/minute, the rms of mold level fluctuation increases to ~0.8 mm for higher dithering strokes. The increase of mold level fluctuation (rms) is almost uniform when casting speed increases from 0.6 to 1.0 m/minute and from 1.0 to 1.4 m/minute, for each of the dithering strokes. Specifically, average mold fluctuations increase from ~0.7 to ~0.85 mm (rms) when increasing steady-state casting speed from 1.0 to 1.4 m/minute (40 to 55 ipm), with a 14-mm dithering stroke.

Conclusions

This work applies plant measurements and computational models to investigate the effect of slidegate dithering on mold level fluctuations. Two different systems of models have been developed, validated separately and applied to capture the different physics occurring in this complicated real-world problem. Both a complex 3D transient turbulent flow CFD model and a simple analytical model have been constructed to investigate the transient variations of flow pattern change, evolution of the slag/steel interface, and average mold level fluctuations during the dithering of slidegate for different operating conditions. A novel, free-surface tracking model with a dynamic mesh technique was created utilizing the dynamic mesh feature of the commercial finite volume method CFD package ANSYS-FLUENT. From the results of both models, the following conclusions can be drawn:

- The new free-surface tracking methodology was proven to be a promising approach to model both transient and steady-state behavior

of the slag/steel interface in terms of accuracy, computational efficiency and applicability to complex multi-phase flow problems, including severe sloshing.

- Severe mold sloshing occurs when the dithering frequency matches the natural frequency of the mold, which is determined only by the mold dimensions.
- The critical sloshing frequency is 0.9 Hz for the 1,840-mm mold width studied here and decreases with increasing width.
- The mechanism of sloshing and its detailed behavior is revealed by the simulation results, where the gravity wave periodically is energized by the increase of liquid steel jet momentum during the dithering cycle, resulting in the magnification of surface waves and mold level fluctuations.
- The average mold level fluctuation can be calculated accurately using a simple analytical model developed in this work, as long as there is no severe sloshing.
- Increasing casting speed during dithering increases the magnitude of the mold level fluctuations. Specifically, average mold level fluctuations increase from ~0.7 to ~0.9 mm (rms) or ~2.0 to ~2.4 mm (peak to valley) when increasing steady-state casting speed from 1.0 to 1.4 m/minute (40 to 55 ipm), with a 14-mm dithering stroke. Thus, casting speed should be restricted when casting wide slabs (e.g., 1,840 mm or 72.5 inches), especially with high dithering stroke.
- Increasing dithering stroke also increases the mold level fluctuations. Specifically, average mold level fluctuations increase from ~0.3 to ~0.7 mm (rms) or ~0.8 to ~2.0 mm (peak to valley) when dithering stroke changes from 6 to 14 mm for the casting speed of 1.0 m/minute (40 ipm), but ~0.4 to ~0.8 mm (rms) or ~1.0 to ~2.4 mm (peak to valley) for the casting speed of 1.4 m/minute (50 ipm). Thus, dithering strokes larger than 12 mm should be avoided for casting speeds above 1.0 m/minute (40 ipm) for wide slabs.

Acknowledgments

The authors thank the members of the Continuous Casting Consortium at the University of Illinois at Urbana-Champaign and the National Science Foundation (Grant CMMI-11-30882) for support of this research. The authors also thank Hongbin Yin, Kai Zheng and Bill Umlauf at ArcelorMittal Global R&D in East Chicago for providing the mold level measurement data.

References

1. R. Liu, B.G. Thomas, B. Forman and H. Yin, "Transient Turbulent Flow Simulation With Water Model Validation and Application to Slidegate Dithering," *AISTech Conference Proceedings*, 2012, Vol. I, p. 1317.
2. L.C. Hibbeler, R. Liu and B.G. Thomas, "Review of Mold Flux Entrainment Mechanisms and Model Investigation of Entrainment by Shear-Layer Instability," *7th ECCO*, Düsseldorf, Germany, 2011.
3. S.F. Graebe, G.C. Goodwin and G. Elsley, "Control Design and Implementation in Continuous Steel Casting," *IEEE Control Systems Magazine*, 1995, Vol. 15, No. 8, p. 64.
4. R. de Keyser, "Improved Mold-Level Control in a Continuous Steel Casting Line," *Control Engineering Practice*, 1997, Vol. 5, No. 2, p. 231.
5. Q. Liu and W. Wang, "A Mold Level Mechanism Model in Continuous Casting With Application to Suppression of Limit Cycle," *ACTA AUTOMATICA SINICA*, 2002, Vol. 28, No. 3, p. 156.
6. C.W. Hirt and B.D. Nichols, "Volume of Fluid (VOF) Method for the Dynamics of Free Boundaries," *Journal of Computational Physics*, 1981, Vol. 39, p. 201.
7. H. Lamb, *Hydrodynamics*, Dover Publications, 6th Edition, 1932.
8. A. Prosperetti, "Motion of Two Superposed Viscous Fluids," *Physics of Fluids*, 1981, Vol. 24, No. 7, p. 1217.
9. F.R. Menter, "Two-Equation Eddy-Viscosity Turbulence Models for Engineering Applications," *AIAA Journal*, 1994, Vol. 32, No. 8, p. 1598.
10. P.R. Spalart, W.H. Jou, M. Strelets and S.R. Allmaras, "Comments on the Feasibility of LES for Wings and on the Hybrid RANS/LES Approach," *Proc. of the 1st AFOSR Int. Conf. on DNS/LES*, Arlington, Texas, 1997.
11. R. Liu and B.G. Thomas, "Slidegate Dithering Effects on Transient Flow and Mold Level Fluctuations," *Continuous Casting Consortium Report*, Urbana, Ill., 2012.
12. S. Muzaferija and M. Perić, "Computation of Free-Surface Flows Using the Finite-Volume Method and Moving Grids," *Numerical Heat Transfer, Part B: Fundamentals*, 1997, Vol. 32, No. 4, p. 369.
13. Fluent, ANSYS Inc., User Manual, 2011. ♦

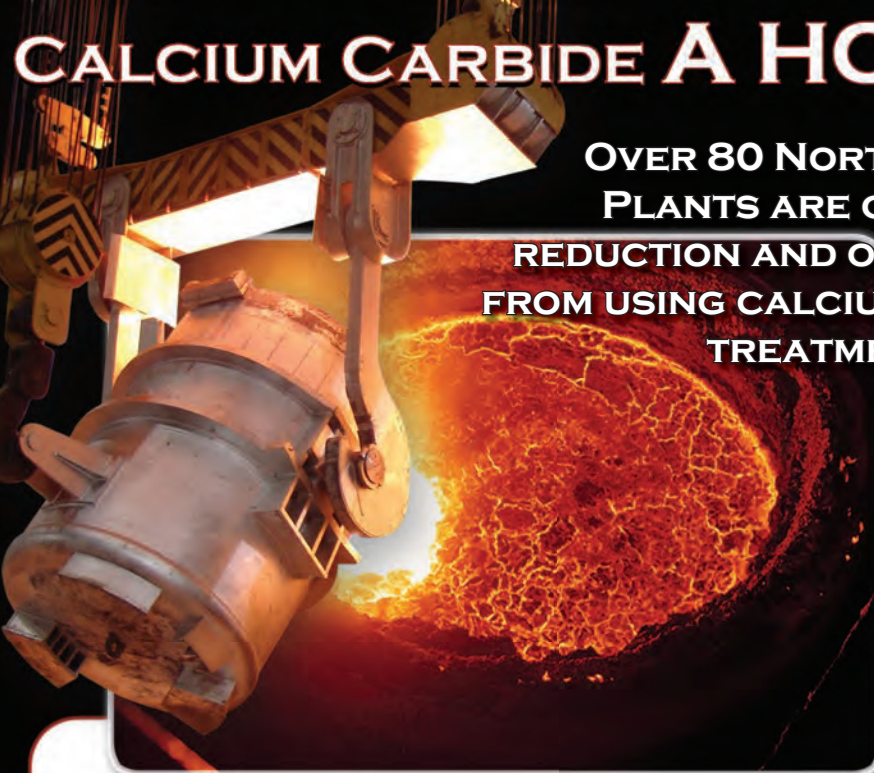


Nominate this paper

Did you find this article to be of significant relevance to the advancement of steel technology? If so, please consider nominating it for the AIST Hunt-Kelly Outstanding Paper Award at AIST.org/huntkelly.

This paper was presented at AISTech 2013 — The Iron & Steel Technology Conference and Exposition, Pittsburgh, Pa., and published in the Conference Proceedings.

CALCIUM CARBIDE A HOT TOPIC



OVER 80 NORTH AMERICAN STEEL PLANTS ARE OBTAINING THE COST REDUCTION AND OPERATING BENEFITS FROM USING CALCIUM CARBIDE FOR THE TREATMENT OF STEEL SLAGS

- CLEANER STEEL
- LESS ALUMINUM FADE
- REFRACTORY PROTECTION
- REDUCE THERMAL LOSSES
- LOWER ELECTRODE CONSUMPTION
- LOWER DEOXIDIZER CONSUMPTION

CALL US AT **CARBIDE INDUSTRIES LLC**, NORTH AMERICA'S PREMIER PRODUCER OF CALCIUM CARBIDE AND LET US SHOW YOU HOW YOU CAN BENEFIT

Toll Free: 800-626-2578 • Fax: 502-775-4200 • E-mail: sales@carbideinc.com

